A Review of Recent Studies on Two-Frequency RF Field-Induced Single-Surface Multipactor Discharge

Asif Iqbal, *Member, IEEE*, Patrick Y. Wong, *Member, IEEE*, De-Qi Wen, *Member, IEEE*, John P. Verboncoeur, *Fellow, IEEE*, and Peng Zhang, *Senior Member, IEEE*

***Abstract*— This article briefly reviews the theory and modeling of single-surface multipactor discharge on a dielectric, focusing on recent studies on two-frequency RF-field-induced multipactor. A novel multiparticle Monte Carlo simulation model with adaptive time steps is used to investigate the time-dependent physics of multipactor discharge. Two-frequency RF operation is found to be effective in reducing multipactor strength compared with single-frequency RF operation with the same total RF power. Strong multipactor mitigation is also demonstrated for nonsinusoidal RF fields of multiple frequencies. Migration of multipactor trajectory is shown for different configurations of the two-frequency RF field. Frequency-domain analysis shows that multipactor-induced normal surface charging electric field consists of only even harmonics of the RF frequency for single-frequency RF operation, but is dominated by strong intermodulation products of the RF carrier frequencies for two-frequency RF operation.**

***Index Terms*— Frequency-domain analysis, Monte Carlo (MC), multipactor, nonsinusoidal waveform, time-dependent physics, two-frequency.**

I. Introduction

MULTIPACTOR discharge [1]–[7] is a nonlinear phenomenon in which electrons driven by a high-frequency RF field create an avalanche by impacting one or more metallic or dielectric surfaces. The electron avalanche sustains itself by an exponential charge growth through secondary electron emission [8]–[11] from the surfaces. If this avalanche of electrons reaches a sufficiently high saturation level [2], [4], [5] by inducing appreciable outgassing from the surface, it can eventually turn into a gaseous-like discharge within the desorbed gas layer, which is called flashover [12].

Manuscript received April 1, 2021; revised August 24, 2021; accepted October 6, 2021. Date of publication October 19, 2021; date of current version November 18, 2021. This work was supported in part by the Air Force Office of Scientific Research (AFOSR) Multidisciplinary University Research Initiative (MURI) Grant FA9550-18-1-0062 and Grant FA9550-21-1-0367, and in part by MSU Foundation Strategic Partnership Grant. The review of this article was arranged by Senior Editor S. J. Gitomer. *(Corresponding author: Peng Zhang.)*

Asif Iqbal, Patrick Y. Wong, and Peng Zhang are with the Department of Electrical and Computer Engineering, Michigan State University, East Lansing, MI 48824 USA (e-mail: iqbalas3@egr.msu.edu; wongpat3@egr.msu.edu; pz@egr.msu.edu).

De-Qi Wen is with the Department of Computational Mathematics Science and Engineering, Michigan State University, East Lansing, MI 48824 USA (e-mail: wendeqi@msu.edu).

John P. Verboncoeur is with the Department of Computational Mathematics Science and Engineering and the Department of Electrical and Computer Engineering, Michigan State University, East Lansing, MI 48824 USA (e-mail: johnv@egr.msu.edu).

Color versions of one or more figures in this article are available at https://doi.org/10.1109/TPS.2021.3118919.

Digital Object Identifier 10.1109/TPS.2021.3118919

While there are some beneficial aspects of multipactor discharge [3], such as vacuum conditioning or electron sources, it is considered detrimental to RF systems in most applications. The discharges may cause breakdown of dielectric windows [13]–[16], erosion of metallic structures, melting of internal components, and perforation of vacuum walls [2]. Multipactor can also detune RF systems, limit the delivery of RF power, and cause a local pressure rise due to the desorption of surface gases [17]. In some cases [18], [19], the multipactor can induce a glow discharge below the expected minimum pressure for a multipactor-free, Paschen-type RF glow discharge [20]. Due to its various undesired effects, multipactor has been a major concern for high-power microwave (HPM) sources [21]–[26], RF accelerators [15], and space-based communication systems [27]–[37].

To date, theoretical and experimental multipactor investigations have heavily focused on multipactor discharge induced by a single-frequency RF field. However, many modern communication systems use multicarrier RF transmission [38], [39]. In addition, modern satellites and spacecraft extensively perform complex multifrequency communication through restricted frequency spectrum [36]. Due to restricted availability of orbital slots, several advanced communication missions are being frequently incorporated in a single satellite payload rendering multifrequency communication essential [40]. Incidental superposition of multiple frequencies can also occur in many RF components due to coupling between imperfectly isolated subsystems, such as in transmission lines and supporting components. Therefore, it is imperative to understand multipactor discharge with multifrequency RF fields.

In this article, we review recent studies conducted at Michigan State University on single-surface dielectric multipactor discharge induced by two-frequency RF fields [41]. The discharge is modeled using a novel multiparticle Monte Carlo (MC) simulation scheme [42]. We start with a mini historical review of studies on single- and multifrequency RF-field-induced single-surface multipactor discharge (Section II). We would like to point out that it is not our intention to give a comprehensive review of multipactor; rather, to provide essential background information for the later discussion. Next, we present the modeling setup for single-surface multipactor with two-frequency RF field and the multiparticle MC model (Section III). The time-dependent physics and the frequency-domain analysis of multipactor discharge are presented in Sections IV and V, respectively. In Section VI, we discuss multipactor mitigation with

nonsinusoidal RF electric fields. Finally, we conclude the article by noting a few aspects of future research in Section VII.

II. Mini Historical Review

A. Multipactor Discharge on a Single Surface

Multipactor discharge was first reported in the 1920s by French physicists C. Gutton and H. Gutton [43]. The first conceptual description of multipactor phenomenon in American technical literature was given in 1934 by Farnsworth [1] who first referred to this phenomenon as "multipactor" and received several patents on technologies which highlighted multipactor discharges [44]–[47]. In 1936, Henneburg *et al.* [48] derived the resonance condition for two-surface multipactor on the transit time for electrons emitted with zero initial velocity. In the 1940s, while investigating high-frequency gas discharges at low pressure, Gill and von Engel [49] rediscovered multipactor and conducted many theoretical and experimental studies on it. In 1950s, Hatch and Williams [6], [7] reformulated the theory within a more concise mathematical framework.

Research on multipactor discharge during this period heavily focused on two surface multipactors and investigation on single-surface multipactor was scarce. However, in his 1961 publication, Vaughan [14] described two types of experimentally observed dielectric window failure in magnetrons and klystrons, namely, cracking and puncturing, and attributed these failures to the electrostatic charging of an evaporated metallic deposit on the surface and an internal multipactor discharge, respectively. In the same year, Preist and Talcott [13] suggested that the dielectric window failure in microwave tubes could be attributed to excessive heating caused by "electron bombardment." They proposed a theory and outlined the necessary conditions for such dielectric failure to take place which was essentially the first theoretical treatment of single-surface multipactor. In the late 1990s, Kishek *et al.* expanded on their theory and conducted a comprehensive study [4], [50] on the topic.

The theory of multipactor discharge on single dielectric surface has been extensively researched since the 1980s. Notable numerical investigations were carried out using MC particle simulations [3], [5], [39] and particle-in-cell (PIC) simulations [51]. The classical analytical theory based on electron kinetics has been used to study the single-surface multipactor susceptibility diagram [4] and power deposition onto the dielectric [52]. The effects of space charge [53], [54], external electric and magnetic fields [5], [55], [56], oblique RF electric fields [56], [57], wave reflection [55], and desorption or background gases [5], [58] have been investigated. The transition of window breakdown from vacuum multipactor discharge to RF plasma has been studied, by both PIC simulations [51] and volume-averaged global models (GMs) [59], [60]. Analytical scaling laws have been derived for dielectric window breakdown in vacuum and collisional regimes [61]. Time-dependent physics of single surface multipactor has been investigated [62].

In 2010, Anza *et al.* [28] proposed the nonstationary statistical theory for both two-surface and single-surface multipactor. Recently, Siddiqi and Kishek [63] have proposed a map-based theory based on principles from nonlinear dynamics and chaos theory to study multipactor discharge. The theory has been used to study multipactor stability and growth [64] and to obtain susceptibility charts [65].

B. Multipactor Under Multicarrier RF Operation

To date, a majority of the studies on multicarrier RF-field-induced multipactor discharge have been carried out for two-surface geometry. The industry has widely adopted semiempirical multipaction threshold prediction methods [66] and nonempirical and conservative approaches [67] to tackle multicarrier multipactor discharge for parallel plate waveguides, including the most commonly used "20 gap crossing rule" [30]. Anza *et al.* [29], [31] generalized the nonstationary statistical theory for multicarrier signals. Wong *et al.* [36] recently proposed a model to assess the effects of multipactor on the distortion of a signal for planer and coaxial geometry. They also proposed a novel way of using multipactor discharges for harmonic generation [68] using the intrinsic phase-focusing mechanism of multipactor as a natural charge-bunching mechanism. Hubble *et al.* [35], [69] studied multipactor under two-tone and multicarrier RF operations in microstrip geometry and proposed useful improvements in multipactor testing and diagnostics [70]–[72]. In addition, several studies have been conducted on the frequency-domain analysis of two-surface multipactor discharge [73]–[76].

Multicarrier operation has also been found effective for multipaction mitigation. Semenov *et al.* [38] showed in the early 2000s that with two-frequency RF operation, mitigation of multipactor breakdown can be achieved in a metallic gap when the two carrier waves have close but separated frequencies. Using the two-frequency RF field, Rice and Verboncoeur [77] demonstrated the migration of multipactor trajectories to specific desirable locations in the parallel plate geometry for the purpose of cleaning the structure or reducing multipactor susceptibility.

For single-surface geometry, we note Siddiqi and Kishek's [78] investigation of single-surface susceptibility diagrams for two-frequency RF field using the map-based theory.

III. Modeling Single-Surface Multipactor With Two-Frequency RF Field

A. Electron Kinetics Modeling Setup

The multipactor electrons are subjected to forces imposed by the RF electric field $E_y = [E_{\mathrm{RF}} \sin(\omega t + \theta) + \beta E_{\mathrm{RF}} \sin(n(\omega t + \theta) + \gamma)]$ acting along the y-direction and the normal electric field E_x originating from the residual charge on the dielectric acting along the x-direction (Fig. 1). Here, E_{RF} is the peak electric field strength, ω is the angular frequency, and θ is the initial phase of the electric field of the fundamental carrier mode. β is the field strength of the second carrier mode relative to the fundamental mode, n is the ratio of the frequencies of the two carrier modes, and γ is the relative phase of the second carrier mode. The flight trajectory of a multipactor electron is governed by the force law [4], from which we can obtain the instantaneous velocities and positions of the multipactor electrons as well as their impact energies and angles [79].

The secondary electron yield (SEY), δ, defined as the average number of secondary electrons produced by the impact of each primary electron upon the surface, is a function of the impact energy of the primary electron, E_i, and the angle to the surface normal, ξ, at which it strikes the surface [10]. It also depends on material properties, i.e., the maximum

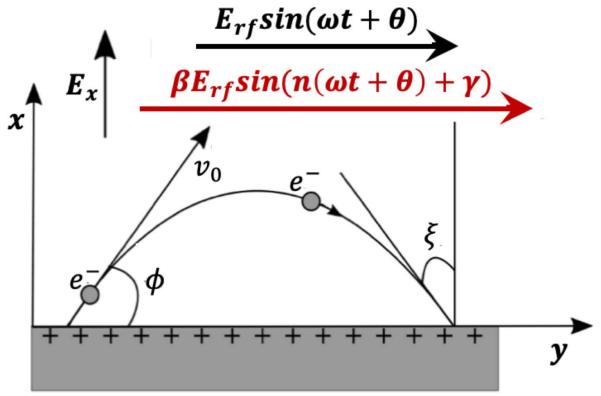

Fig. 1. Schematic of the single-surface multipactor discharge on a dielectric in a normal electric field and a two-frequency parallel RF field. Reproduced from [81] with the permission of IEEE.

yield, $\delta_{\max}$, and the energy at which it occurs, $E_{\max}$. We adopt Vaughan's [10], [80] empirical formula to estimate the SEY. Two values of impact energy, termed the first and second crossover points, E_1 and E_2, respectively, result in a yield of 1, with $\delta > 1$ in between.

B. Multiparticle MC Model

Kishek *et al.* [3], [4] first used a single macroparticle MC simulation approach for analyzing single-surface multipactor susceptibility boundaries. In this approach, electrons emitted from the surface are considered to be clumped together in a single macroparticle. Upon its impact on the surface, the charge and mass of the macroparticle are updated according to the SEY (δ) of the impact. In a given ($E_{\rm RF}$, E_x) parameter regime, boundaries of multipactor susceptibility are determined when the average SEY over N impacts becomes 1, i.e., $\bar{\delta} = (\delta_1.\delta_2, \ldots, \delta_N)^{1/N} = 1$. The single macroparticle MC model has been effective in constructing the susceptibility diagram [4], [5], [41]. However, it showed significant limitations in resolving the time-dependent physics of single-surface multipactor, producing low-resolution temporal profiles of the RF ($E_{\rm RF}$) and the normal (E_x) electric fields, as well as the SEY (δ) (see Fig. 5 of [52]).

To overcome the limitation of the single-particle MC simulation, Kim and Verboncoeur [62] adopted a variable number of particles' approach, where the number of particles is varied in the simulation while the charge per particle is kept fixed. This allows for better statistics in a growing discharge, but is relatively computationally costly, as the fixed time steps have to be set small compared with the time of flight of the particles between subsequent bounces on the surface [62].

To tackle these limitations, we introduced the novel multiparticle MC model [42] where the simulation consists of a fixed number of macroparticles throughout the simulation. Each macroparticle is assigned the same amount of initial negative charge. For charge neutrality, the total charge contained in the macroparticles is equal to the total positive surface charge, which produces the corresponding surface charging field E_x. We follow the trajectory of these macroparticles over a large number (N) of impacts in an MC simulation. Each iteration of the MC simulation tracks one impact of a macroparticle onto the surface, upon which the charge and mass of the impacting macroparticle and the normal electric field (E_x) are updated according to the SEY and Gauss' law, respectively, while the charge and mass of the other macroparticles in flight remain unchanged by the impact. The temporal profiles of E_y, E_x, and δ are obtained by converting the iteration number N into the scale of time using the transit times $\tau_{\min,i}$ for each iteration.

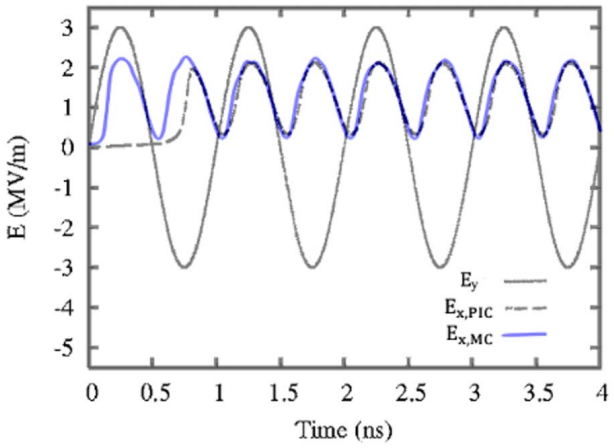

Fig. 2. Temporal profiles of the normal electric field E_x for RF electric field amplitude $E_{\rm RF} = 3$ MV/m and RF frequency $f_{\rm RF} = 1$ GHz from PIC simulation [62] (dashed black line) and multiparticle MC simulation (blue solid line) [42]. The results from MC simulations match almost exactly with that of PIC simulation. We use $N = 50$ macroparticles in MC simulation [79].

The multiparticle MC approach captures the statistics better than the single-particle approach. Since the number of macroparticles is fixed in this model, it still offers a simpler and less costly implementation than the variable number of particles approach or PIC simulation. More importantly, the time intervals between subsequent bounces of different macroparticles on the surface are calculated *exactly*.

It is noteworthy that though space charge effects are not considered in the multiparticle MC model, Fig. 2 demonstrates that the temporal profiles of E_x obtained from the PIC simulation of Kim and Verboncoeur (Fig. 2(b) of [62]) which accounts for space charge effects and from our multiparticle MC technique (Fig. 2(a) of [42]) match almost exactly, for the special case of RF electric field amplitude $E_{\rm RF} = 3$ MV/m and RF frequency $f_{\rm RF} = 1$ GHz. In Fig. 3(a)–(c), excellent agreement is also observed between the instantaneous normal electric field (E_x) profiles obtained from the multiparticle MC and PIC simulations [57], [82] for three different cases of two-frequency RF-field-induced multipactor. This indicates that the effects of space charge may not be significant for the parameter space explored in this study. A detailed examination on the effects of space charge on single-surface multipactor dynamics and susceptibility is needed for future research.

IV. Time-Dependent Physics

It is understood [4], [39], [42] that the ac saturation for a given RF amplitude, where the normal surface charging field reaches a time-averaged saturation value and the temporal relationship between the fields normal and parallel to the surface traces a closed Lissajous curve [62], occurs at the lower multipactor susceptibility boundary. For instance, for the RF amplitude $E_{\rm RF} = 3$ MV/m and the total transmitted RF power per unit area $\bar{P}_{\rm RF} = c\epsilon|E_{\rm RF}|^2/2 = 1.2 \times 10^{10}$ W/m^2, the ac saturation occurs at point "A" of Fig. 4(a) with the normal electric field $E_x = 0.93$ MV/m. This is very close to the time-averaged value of $E_x(t)$ of 0.9 MV/m obtained from Fig. 4(b).

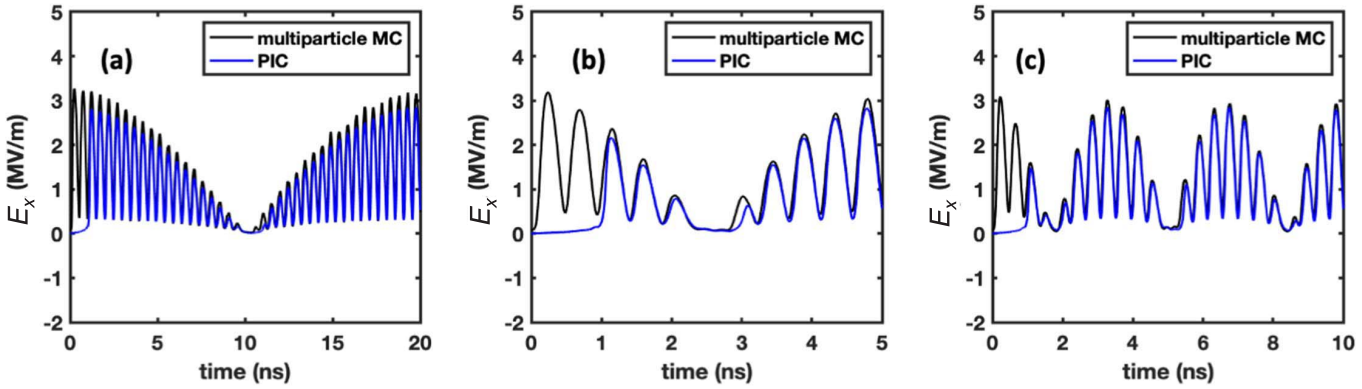

Fig. 3. Instantaneous normal electric field, E_x, for two-frequency RF fields with carrier frequencies (a) $f_1 = 1$ GHz and $f_2 = 1.05$ GHz, (b) $f_1 = 1$ GHz and $f_2 = 1.20$ GHz, and (c) $f_1 = 1$ GHz and $f_2 = 1.30$ GHz obtained from multiparticle MC simulation (black lines) and PIC simulation [57], [82] (blue lines). We set $\beta = 1$, $\gamma = 0$, and $E_{\mathrm{RF}} = 3$ MV/m in the calculation. We use $N = 50$ macroparticles in MC simulation [79].

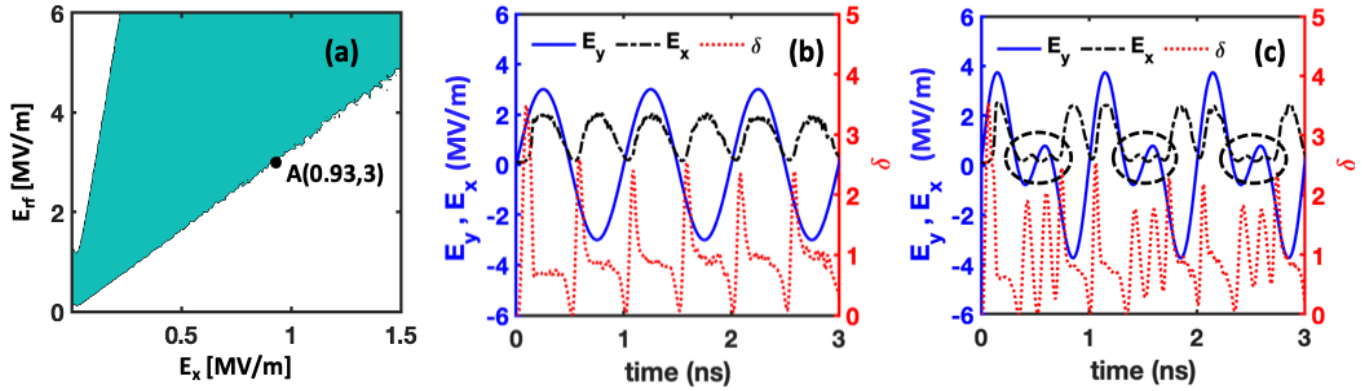

Fig. 4. (a) Multipactor susceptibility boundaries obtained from single-particle MC simulation in the (E_x, E_{RF}) plane with single-frequency RF field. The cyan region shows the parameter regime where the multipactor discharge develops. (b) and (c) Instantaneous RF electric field, E_y (solid blue lines), normal electric field, E_x (broken black lines), and SEY, δ (dotted red lines), for (b) single-frequency RF field, $\beta = 0$ and $E_{\mathrm{RF}} = 3$ MV/m, and (c) two-frequency RF field, $n = 2$, $\beta = 1$, $\gamma = 0$, and individual carrier amplitude $E_{\mathrm{RF}} = 3/\sqrt{2}$ MV/m obtained from multipactor MC simulation. The average SEY $\delta_{\mathrm{avg}} = 1$ in the saturation regime. We use a fundamental RF frequency, $f_{\mathrm{RF}} = 1$ GHz, $\delta_{\mathrm{max0}} = 3$, $E_{\mathrm{max0}} = 420$ eV, and $E_{0m}/E_{\mathrm{max0}} = 0.005$ in all the calculations. Reproduced from [79] and [81] with the permission of IEEE and American Physical Society (APS).

For a single-frequency RF electric field, it is found [42], [62], [79] that the temporal profile of the normal electric field E_x oscillates at twice the RF frequency in the ac saturation state, as shown in Fig. 4(b). With the addition of the second carrier mode, the overall RF electric field becomes periodically modulated, which is expected to distort the electrons' trajectory, leading to modified multipactor dynamics [42]. For instance, in Fig. 4(c) with $n = 2, \beta = 1$, and $\gamma = 0$, the temporal profiles of the SEY δ and normal electric field E_x oscillate at four times the RF frequency [42]. Consequently, the normal surface charging field, E_x [broken black curve in Fig. 4(c)], which corresponds to the multipactor strength in the system stays at a lower value [broken black circled regions in Fig. 4(c)] for a longer duration during an RF period. The resulting time-averaged saturation value of E_x becomes lower (~ 0.75 MV/m) compared with that with single-frequency RF field with the same total RF power $\bar{P}_{\mathrm{RF}}$ [79]. Therefore, two-frequency RF operation reduces multipactor strength compared with single-frequency RF operation with the same total RF power. We also find that multipactor susceptibility is insensitive to γ while the effect of the second carrier mode becomes less prominent as β decreases.

Examination of the multipacting particle trajectories reveals that with a single-frequency RF field acting parallel to the surface (y-direction in Fig. 1), the mean horizontal displacement over a complete RF period is negligible. This happens due to the periodic symmetry of the single-frequency RF field in the positive and negative y-direction. However, when a second carrier mode is present in the RF field, the periodic symmetry in the y-direction is typically not present, and consequently, a mean horizontal displacement of the macroparticles takes place over a complete RF period. Fig. 5 shows that for $0 < \gamma < \pi$, the periodic asymmetry of the RF field causes a mean horizontal displacement of the macroparticles in the $-y$-direction and the maximum horizontal displacement occurs for $\gamma = \pi/2$. On the other hand, for $\pi < \gamma < 2\pi$, a mean horizontal displacement of the macroparticles in the $+y$-direction is observed, and the maximum horizontal displacement occurs for $\gamma = 3\pi/2$. This capability of migrating multipactor trajectories can be of interest to RF system operators in applications such as cleaning a given location in a structure to reduce further susceptibility to multipactor, or for directing multipacting electrons to a specific desirable location in the geometry [77].

The effect of frequency ratio (n) on multipactor susceptibility is negligible [79]. This is evident from Fig. 6(a) where the upper and lower susceptibility boundaries for different frequency ratios (n) are largely overlaid with one another. The reason for this insensitivity can be inferred from the time-dependent physics. We find that for different frequency separations between the two carrier modes, the RF envelopes become different. However, for a given RF amplitude, the

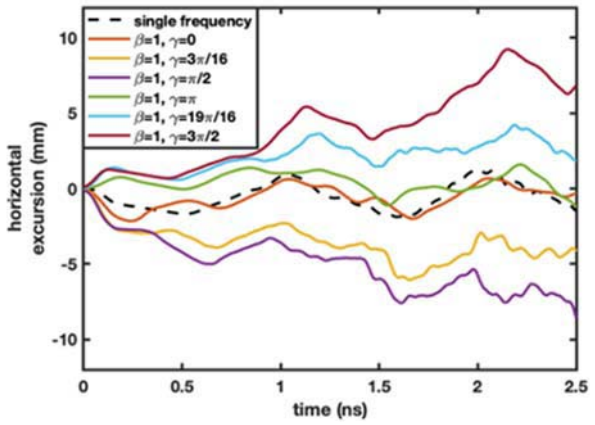

Fig. 5. Comparison of the mean horizontal displacements (along the dielectric surface) for the single- and two-frequency RF electric fields with $f_{\mathrm{RF}} = 1$ GHz,$\theta = 0, n = 2, \beta = 1,$ and $\gamma = 0, 3\pi/16, \pi/2, \pi, 19\pi/16, 3\pi/2$.

time-averaged values of the resulting normal electric fields remain almost the same.

The periodic beating of the RF electric field E_y [blue line in Fig. 6(b)] due to noninteger frequency ratio between the two carrier modes produces beat wave in the temporal profile of the normal surface charging field [broken black curve in Fig. 6(b)] consisting of multiple frequency components [79]. The beat frequency of such waves depends on the frequency separation, $\Delta f = f_2 - f_1$. The frequency components of the normal electric fields are analyzed through the frequency-domain analysis of single-surface multipactor [81].

V. Frequency-Domain Analysis

For the frequency-domain analysis of single-surface multipactor, we first use the fast Fourier transform (FFT) algorithm using MATLAB to obtain the discrete Fourier transform (DFT) (also called the amplitude spectrum) of the temporal profiles of E_x in the ac saturation state. We conduct our analysis for both single- and two-frequency RF-field-induced multipactor. To our knowledge, this is the first study conducted on the frequency-domain analysis of single-surface multipactor.

In the amplitude spectrum of E_x for single-frequency RF-field-induced multipactor [Fig. 7(a)], the first spectral peak appears at frequency $f = 0$ which corresponds to the time-averaged value of E_x in the ac saturation state [corresponding to point "A" in Fig. 4(a)]. Spectral peaks also appear at even harmonics of the RF frequency, $2lf_{\mathrm{RF}}$, where l is a positive integer. The absence of odd harmonics of the RF frequency in E_x is expected. Because surface charging due to multipactor discharge from the dielectric surface is independent of the direction (i.e., either positive or negative) of the parallel RF electric field E_{RF}, the normal surface charging field E_x must be symmetric in the positive and negative half cycles of E_{RF}.

The heights of the spectral peaks are almost independent of the RF frequency, f_{RF}, and proportional to the RF amplitude, E_{RF}. Therefore, the relationship between the spectral peak heights and the RF amplitude can be expressed with a linear empirical equation [81]. The temporal profiles of the normal electric field can be approximated with a simple empirical equation in terms of the DFT peaks as well [81]. Our empirical fitting coefficients presented in [81] remain applicable to new cases.

In the amplitude spectrum of E_x for two-frequency RF-field-induced multipactor [Fig. 7(b)], we observe spectral peaks at various frequencies of intermodulation products of the carrier frequencies ($f_{1,2}$). Pronounced peaks are observed at the sum and difference frequencies of the carrier frequencies, at multiples of those frequencies, and at multiples of the individual carrier frequencies. Similar to the single-frequency RF-field-induced multipactor case, the relationship between the heights of the spectral peaks and the RF amplitude can be fit with a linear equation [81]. An empirical equation has also been derived to approximate the temporal profiles of the normal electric field in terms of the most prominent DFT peaks [81].

VI. Nonsinusoidal RF-Field-Induced Single-Surface Multipactor

In this section, we briefly discuss our study on single-surface multipactor discharge with a Gaussian shape RF electric field, $E_y = E_{\mathrm{RF}}\{\exp[-\beta(t-t_1)^2] - \exp[-\beta(t-t_2)^2]\}$; $nT_{\mathrm{RF}} \leq t < (n+1)T_{\mathrm{RF}}$. Here, E_{RF} is the field amplitude, and $t_1 = (n+0.25)T_{\mathrm{RF}}$ and $t_2 = (n+0.75)T_{\mathrm{RF}}$ are the times of the field maximum and minimum, respectively, with n being an integer and T_{RF} the RF period. β corresponds to the half peak widths, $\Delta\tau = 2(\ln 2/\beta)^{1/2}$, of the field. Fig. 8(a) shows the temporal profiles of the RF electric fields of sinusoidal and Gaussian form for different values of $\Delta\tau$ with the same average RF power, $\bar{P}_{\mathrm{RF}} = 1.2 \times 10^{10}$ W/m^2.

We previously observed in Section IV that for single- and two-frequency RF operations with $\bar{P}_{\mathrm{RF}} = 1.2 \times 10^{10}$ W/m^2, the time-averaged saturation values of the normal electric field are $E_{x,\mathrm{avg}} \sim 0.9$ MV/m and $E_{x,\mathrm{avg}} \sim 0.75$ MV/m, respectively. However, with Gaussian-type RF field with the same $\bar{P}_{\mathrm{RF}}$, we find that for $0.05 \leq \Delta\tau/T_{\mathrm{RF}} \leq 0.15$, $E_{x,\mathrm{avg}}$ is reduced by at least a factor of 2 up to an order of magnitude compared with those for the sinusoidal cases [Fig. 8(b)] [82]. The reason for this reduction in multipactor strength can be explained from the time-dependent physics [82]. Due to the larger RF field peak values at $t = t_1$ and $t = t_2$, the electrons in flight gain more energy during these times in an RF period. However, as the half peak width $\Delta\tau$ decreases, the energy gained by emitted electrons from the RF field and consequently the impact energies of the electrons also decrease. As a result, the time-averaged values of the SEY and the normal electric field are significantly reduced for RF field with smaller half peak width.

Since Gaussian-type RF field is intrinsically a multifrequency waveform, which is shown to be well-represented by an RF field consisting of only five frequency components [82], this key result demonstrates that multicarrier RF fields may be helpful in the design of agile RF waveshapes to mitigate single-surface multipactor discharge.

VII. Conclusion

In light of the growing importance of multicarrier RF operation in RF systems and devices as well as in space applications, this article attempts to collate recent studies on single-surface multipactor discharge induced by RF fields with two carrier frequencies. Two-frequency RF operation has been found to be useful in multipactor suppression and also in controlling the migration of multipactor trajectories in a given geometry. Frequency components associated with single-surface multipactor discharge for single- and two-frequency RF operation have been analyzed.

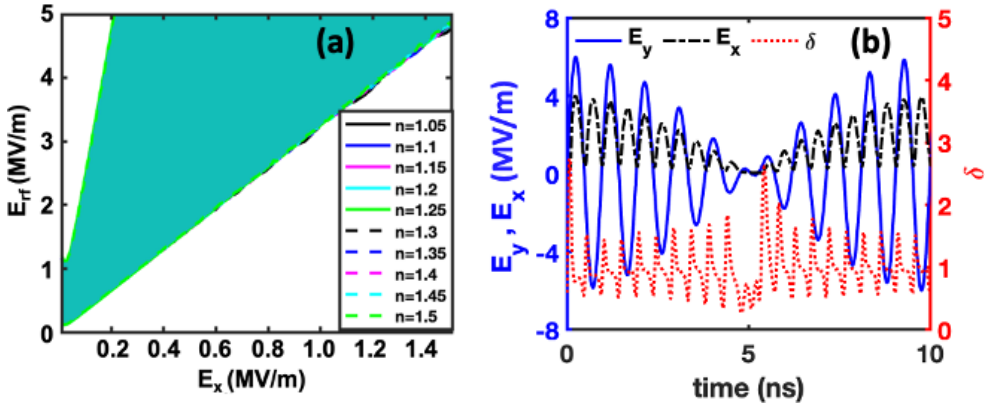

Fig. 6. (a) Multipactor susceptibility diagrams for two-frequency RF fields with $\beta = 1$, $\gamma = 0$, and frequency ratio $1.05 \le n \le 1.5$. The cyan region shows the parameter regime where the multipactor discharge develops. The upper and lower susceptibility boundaries for different frequency ratios n are largely overlaid with one another. (b) Instantaneous RF electric field, E_y (solid blue lines), normal electric field, E_x (broken black lines), and SEY, δ (dotted red lines), for two-frequency RF field, $f_1 = 1$ GHz and $f_2 = 1.1$ GHz obtained from multiparticle MC simulation. The average SEY $\delta_{\text{avg}} = 1$ in the saturation regime. We set $\beta = 1$, $\gamma = 0$, and $E_{\text{RF}} = 3$ MV/m in the calculation. Reproduced from [79] with the permission of APS.

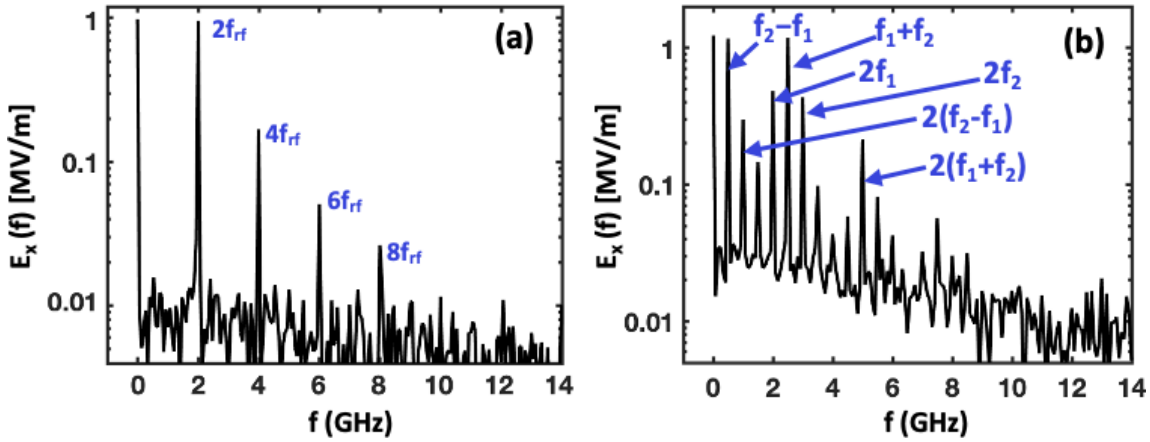

Fig. 7. Amplitude spectrum of the normal electric field in the ac saturation state induced by: (a) single-frequency RF field with amplitude $E_{\text{RF}} = 3$ MV/m and frequencies $f_{\text{RF}} = 1$ GHz. Pronounced spectral peaks are observed at even harmonics of the RF frequency. (b) Two-frequency RF field with individual carrier amplitude $E_{\text{RF}} = 3$ MV/m (with $\beta = 1$) and carrier frequencies $f_1 = 1$ GHz and $f_2 = 1.5$ GHz. Pronounced spectral peaks are observed at frequencies $(f_2 \pm f_1)$, $2f_{1,2}$, and $2(f_2 \pm f_1)$. Reproduced from [81] with the permission of IEEE.

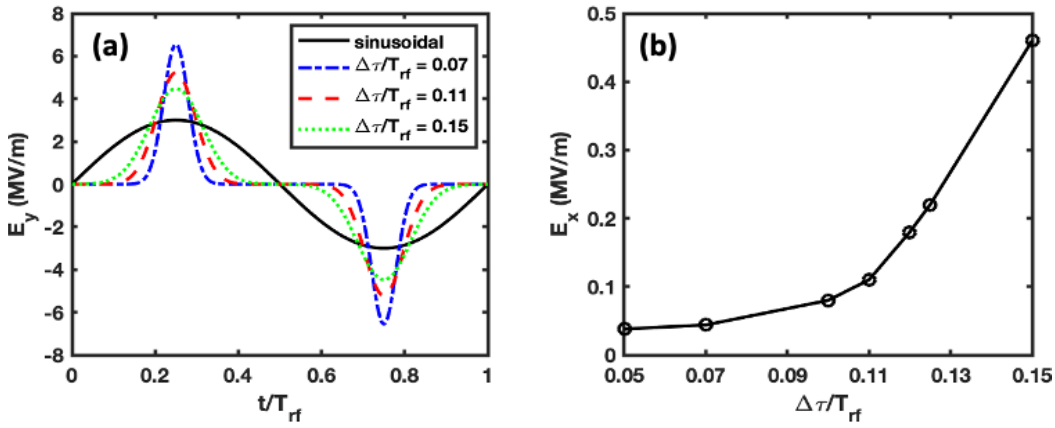

Fig. 8. (a) Temporal profiles of the RF electric fields of sinusoidal and Gaussian form for $\Delta\tau/T_{\text{RF}} = 0.07, 0.11$, and 0.15 with the same total RF power, $\bar{P}_{\text{RF}} = 1.2 \times 10^{10}$ W/m^2. (b) Time-averaged saturation value of the normal electric field E_x with different Gaussian RF fields with the same total RF power, $\bar{P}_{\text{RF}} = 1.2 \times 10^{10}$ W/m^2, obtained from multiparticle MC simulation versus half peak width of the RF field. Reproduced from [82] with the permission of American Institute of Physics (AIP) publication.

Our ongoing study extends to two-frequency RF-field-induced two-surface multipactor where the effects of the second carrier mode on multipactor susceptibility and the time-dependent physics are explored with and without space charge effect. A detailed account of this study will be presented in a future publication [83].

The scope for future studies remains vast. The time-dependent physics and multipactor susceptibility of multicarrier RF-field-induced single-surface multipactor discharge are still largely unexplored. In particular, multipactor susceptibility charts may be constructed for various nonsinusoidal RF waveforms. Another domain of future research is to explore

multipactor induced by nontransverse RF modes of multiple frequencies, which are expected to significantly change electron impact energies and angles, thus leading to different secondary electron emission conditions.

In our studies presented in this article, we neglected space charge effects. Systematic studies are needed to examine space charge effects in both the secondary electron emission process [54] and the motion of multipactor electrons [53], [84], [85]. Multifrequency multipactor near structured surfaces [86]–[90] may also be studied.

To our knowledge, the frequency components of the surface charging field associated with single-surface multipactor discharge have not been investigated in experiments. Diagnosis and harvesting of these frequency components may be an interesting research pursuit in the future. These frequency components may be useful in various applications, such as harmonic generation [68]. Future research may also include the effect of these frequency components on transmitted RF signal quality [36].

Finally, many recent analytical predictions and simulation results on two-frequency and multicarrier RF-field-induced multipactor discharge are yet to be experimentally validated. Such experimental investigations are expected to further improve our understanding of multipactor under multifrequency operation.

REFERENCES

[1] P. T. Farnsworth, "Television by electron image scanning," *J. Franklin Inst.*, vol. 218, no. 4, pp. 411–444, Oct. 1934.

[2] J. R. M. Vaughan, "Multipactor," *IEEE Trans. Electron Devices*, vol. ED-35, no. 7, pp. 1172–1180, Jul. 1988.

[3] R. A. Kishek, Y. Y. Lau, L. K. Ang, A. Valfells, and R. M. Gilgenbach, "Multipactor discharge on metals and dielectrics: Historical review and recent theories," *Phys. Plasmas*, vol. 5, no. 5, p. 2120, 1998, doi: 10.1063/1.872883.

[4] R. A. Kishek and Y. Y. Lau, "Multipactor discharge on a dielectric," *Phys. Rev. Lett.*, vol. 80, no. 1, p. 193, Jan. 1998, doi: 10.1103/PhysRevLett.80.193.

[5] P. Zhang, Y. Y. Lau, M. Franzi, and R. M. Gilgenbach, "Multipactor susceptibility on a dielectric with a bias DC electric field and a background gas," *Phys. Plasmas*, vol. 18, no. 5, May 2011, Art. no. 053508, doi: 10.1063/1.3592990.

[6] A. J. Hatch and H. B. Williams, "The secondary electron resonance mechanism of low-pressure high-frequency gas breakdown," *J. Appl. Phys.*, vol. 25, no. 4, pp. 417–423, Apr. 1954, doi: 10.1063/1.1721656.

[7] A. J. Hatch and H. B. Williams, "Multipacting modes of high-frequency gaseous breakdown," *Phys. Rev.*, vol. 112, no. 3, p. 681, Nov. 1958.

[8] H. Bruining, J. H. De Boer, and W. G. Burgers, "Secondary electron emission of soot in valves with oxidecathode," *Physica*, vol. 4, pp. 267–275, Apr. 1937, doi: 10.1016/S0031-8914(37)80047-6.

[9] A. J. Dekker, "Secondary electron emission," in *Solid State Physics*, vol. 6, F. Seitz and D. Turnbull, Eds. New York, NY, USA: Academic, 1958, pp. 251–311, doi: 10.1016/S0081-1947(08)60728-6.

[10] J. R. M. Vaughan, "A new formula for secondary emission yield," *IEEE Trans. Electron Devices*, vol. 36, no. 9, pp. 1963–1967, Sep. 1989.

[11] M. Furman and M. Pivi, "Probabilistic model for the simulation of secondary electron emission," *Phys. Rev. Special Topics Accel. Beams*, vol. 5, no. 12, Dec. 2002, Art. no. 124404, doi: 10.1103/PhysRevSTAB.5.124404.

[12] A. A. Neuber, M. Butcher, H. Krompholz, L. L. Hatfield, and M. Kristiansen, "The role of outgassing in surface flashover under vacuum," *IEEE Trans. Plasma Sci.*, vol. 28, no. 5, pp. 1593–1598, Oct. 2000, doi: 10.1109/27.901239.

[13] D. H. Preist and R. C. Talcott, "On the heating of output windows of microwave tubes by electron bombardment," *IRE Trans. Electron Devices*, vol. 8, no. 4, pp. 243–251, Jul. 1961, doi: 10.1109/T-ED.1961.14797.

[14] J. R. M. Vaughan, "Some high-power window failures," *IRE Trans. Electron Devices*, vol. 8, no. 4, pp. 302–308, Jul. 1961, doi: 10.1109/T-ED.1961.14804.

[15] S. Yamaguchi, Y. Saito, S. Anami, and S. Michizono, "Trajectory simulation of multipactoring electrons in an S-band pillbox RF window," *IEEE Trans. Nucl. Sci.*, vol. 39, no. 2, pp. 278–282, Apr. 1992, doi: 10.1109/23.277497.

[16] A. Neuber, J. Dickens, D. Hemmert, H. Krompholz, L. L. Hatfield, and M. Kristiansen, "Window breakdown caused by high-power microwaves," *IEEE Trans. Plasma Sci.*, vol. 26, no. 3, pp. 296–303, Jun. 1998.

[17] T. P. Graves, "Experimental investigation of electron multipactor discharges at very high frequency," M.S. thesis, Dept. Nucl. Sci. Eng., Massachusetts Inst. Technol., Cambridge, MA, USA, 2006. [Online]. Available: https://dspace.mit.edu/handle/1721.1/41284

[18] F. Höhn, W. Jacob, R. Beckmann, and R. Wilhelm, "The transition of a multipactor to a low-pressure gas discharge," *Phys. Plasmas*, vol. 4, no. 4, pp. 940–944, 1997, doi: 10.1063/1.872564.

[19] T. P. Graves, S. J. Wukitch, B. LaBombard, and I. H. Hutchinson, "Effect of multipactor discharge on Alcator C-Mod ion cyclotron range of frequency heating," *J. Vac. Sci. Technol. A, Vac., Surf., Films*, vol. 24, no. 3, pp. 512–516, May 2006, doi: 10.1116/1.2194937.

[20] J. D. Cobine, *Gaseous Conductors*. New York, NY, USA: Dover, 1958. [Online]. Available: https://biblio.co.uk/book/gaseous-conductors-cobine-jd/d/723026587

[21] J. H. Booske, "Plasma physics and related challenges of millimeter-wave-to-terahertz and high power microwave generation," *Phys Plasmas*, vol. 15, no. 5, p. 17, Feb. 2008, doi: 10.1063/1.2838249.

[22] R. J. Barker, N. C. Luhmann, J. H. Booske, and G. S. Nusinovich, *Modern Microwave and Millimeter Wave Power Electronics*. Piscataway, NJ, USA: IEEE Press, 2004.

[23] J. W. Luginsland *et al.*, *High-Power Microwave Sources and Technologies*, E. Schamiloglu and R. J. Barker, Ed. New York, NY, USA: Wiley, 2001, p. 376.

[24] D. Shiffler, T. K. Statum, T. W. Hussey, O. Zhou, and P. Mardahl, *Modern Microwave and Millimeter Wave Power Electronics*, Piscataway, NJ, USA: IEEE Press, 2005, p. 691.

[25] P. Wong, P. Zhang, and J. Luginsland, "Recent theory of traveling-wave tubes: A tutorial-review," *Plasma Res. Exp.*, vol. 2, no. 2, 2020, Art. no. 023001, doi: 10.1088/2516-1067/ab9730.

[26] J. Benford, J. A. Swegle, and E. Schamiloglu, *High Power Microwaves*, 2nd ed. Boca Raton, FL, USA: CRC Press, 2007, doi: 10.1201/9781420012064.

[27] N. Rozario, H. F. Lenzing, K. F. Reardon, M. S. Zarro, and C. G. Baran, "Investigation of Telstar 4 spacecraft Ku-band and C-band antenna components for multipactor breakdown," *IEEE Trans. Microw. Theory Techn.*, vol. 42, no. 4, pp. 558–564, Apr. 1994.

[28] S. Anza, C. Vicente, J. Gil, V. E. Boria, B. Gimeno, and D. Raboso, "Nonstationary statistical theory for multipactor," *Phys. Plasmas*, vol. 17, no. 6, Jun. 2010, Art. no. 062110, doi: 10.1063/1.3443128.

[29] S. Anza *et al.*, "Multipactor theory for multicarrier signals," *Phys. Plasmas*, vol. 18, no. 3, pp. 1–13, 2011, doi: 10.1063/1.3561821.

[30] S. Anza *et al.*, "Multipactor prediction with multi-carrier signals: Experimental results and discussions on the 20-gap-crossing rule," in *Proc. 8th Eur. Conf. Antennas Propag. (EuCAP)*, Apr. 2014, pp. 1638–1642.

[31] S. Anza, C. Vicente, J. Gil, V. E. Boria, and D. Raboso, "Experimental verification of multipactor prediction methods in multicarrier systems," in *Proc. 46th Eur. Microw. Conf. (EuMC)*, Oct. 2016, pp. 226–229.

[32] S. Anza, C. Vicente, B. Gimeno, V. E. Boria, and J. Armendáriz, "Long-term multipactor discharge in multicarrier systems," *Phys. Plasmas*, vol. 14, no. 8, Aug. 2007, Art. no. 082112, doi: 10.1063/1.2768019.

[33] A. Sazontov *et al.*, "Multipactor discharge on a dielectric surface: Statistical theory and simulation results," *Phys. Plasmas*, vol. 12, no. 9, Sep. 2005, Art. no. 093501, doi: 10.1063/1.2011348.

[34] V. E. Semenov, N. Zharova, R. Udiljak, D. Anderson, M. Lisak, and J. Puech, "Multipactor in a coaxial transmission line. II. Particle-in-cell simulations," *Phys. Plasmas*, vol. 14, no. 3, Mar. 2007, Art. no. 033509, doi: 10.1063/1.2710466.

[35] A. A. Hubble, M. S. Feldman, P. T. Partridge, and R. Spektor, "Evolution of multipactor breakdown in multicarrier systems," *Phys. Plasmas*, vol. 26, no. 5, May 2019, Art. no. 053502, doi: 10.1063/1.5087069.

[36] P. Y. Wong, Y. Y. Lau, P. Zhang, N. Jordan, R. M. Gilgenbach, and J. Verboncoeur, "The effects of multipactor on the quality of a complex signal propagating in a transmission line," *Phys. Plasmas*, vol. 26, no. 11, Nov. 2019, Art. no. 112114, doi: 10.1063/1.5125408.

[37] *Special sessions on Multipactor, I and II*, IEEE ICOPS, Denver, CO, USA, Jun. 2018.

[38] V. Semenov, A. Kryazhev, D. Anderson, and M. Lisak, "Multipactor suppression in amplitude modulated radio frequency fields," *Phys. Plasmas*, vol. 8, no. 11, pp. 5034–5039, Nov. 2001, doi: 10.1063/1.1410980.

[39] A. Iqbal, J. Verboncoeur, and P. Zhang, "Multipactor susceptibility on a dielectric with two carrier frequencies," *Phys. Plasmas*, vol. 25, no. 4, Apr. 2018, Art. no. 043501, doi: 10.1063/1.5024365.

[40] F. Piro and Y. Brand, "PIM and multipactor considerations for future high-RF power space missions," in *Proc. 8th Eur. Conf. Antennas Propag. (EuCAP)*, Apr. 2014, pp. 1643–1646, doi: 10.1109/EuCAP.2014.6902102.

[41] A. Iqbal, "Multipactor discharge with two-frequency RF fields," Ph.D. dissertation, Dept. Elect. Comput. Eng., Michigan State Univ., Lansing, MI, USA, 2021.

[42] A. Iqbal, J. Verboncoeur, and P. Zhang, "Temporal multiparticle Monte Carlo simulation of dual frequency single surface multipactor," *Phys. Plasmas*, vol. 26, no. 2, Feb. 2019, Art. no. 024503, doi: 10.1063/1.5084143.

[43] C. Gutton and H. Gutton, "Sur la décharge électrique en haute fréquence," *Comp. Rendus*, vol. 186, no. 303, 1928.

[44] P. T. Farnsworth, "Multipactor," U.S. Patent 2 135 615, 1938.

[45] P. T. Farnsworth, "Multipactor oscillator," U.S. Patent 2 137 528, 1938.

[46] P. T. Farnsworth, "Multipactor oscillator and amplifier," U.S. Patent 2 091 439, 1937.

[47] P. T. Farnsworth, "Multipactor phase control," U.S. Patent 2 071 517, 1938.

[48] W. Henneburg, R. Orthuber, and E. Steudel, "Zur Wirkungsweise des Elektronenvervielfachers," *Z Tech Phys*, vol. 17, no. 4, p. 115, 1936.

[49] E. W. B. Gill and A. von Engel, "Starting potentials of high-frequency gas discharges at low pressure," *Proc. Roy. Soc. Lond. A, Math. Phys. Sci.*, vol. 192, no. 1030, pp. 446–463, Feb. 1948, doi: 10.1098/rspa.1948.0018.

[50] R. A. Kishek, "Interaction of multipactor discharge and RF structures," Ph.D. dissertation, Dept. Nucl. Eng., Univ. Michigan, Ann Arbor, MI, USA, 1997. [Online]. Available: https://search.proquest.com/docview/304356825/abstract/CE61FD55A2B342C2PQ/1

[51] H. C. Kim and J. P. Verboncoeur, "Transition of window breakdown from vacuum multipactor discharge to RF plasma," *Phys. Plasmas*, vol. 13, no. 12, Dec. 2006, Art. no. 123506, doi: 10.1063/1.2403782.

[52] L.-K. Ang, Y. Y. Lau, R. A. Kishek, and R. M. Gilgenbach, "Power deposited on a dielectric by multipactor," *IEEE Trans. Plasma Sci.*, vol. 26, no. 3, pp. 290–295, Jun. 1998.

[53] A. Valfells, J. P. Verboncoeur, and Y. Y. Lau, "Space-charge effects on multipactor on a dielectric," *IEEE Trans. Plasma Sci.*, vol. 28, no. 3, pp. 529–536, Jun. 2000.

[54] K. D. Bergeron, "Theory of the secondary electron avalanche at electrically stressed insulator-vacuum interfaces," *J. Appl. Phys.*, vol. 48, no. 7, pp. 3073–3080, Jul. 1977, doi: 10.1063/1.324077.

[55] A. G. Sazontov and V. E. Nevchaev, "Effects of RF magnetic field and wave reflection on multipactor discharge on a dielectric," *Phys. Plasmas*, vol. 17, no. 3, Mar. 2010, Art. no. 033509, doi: 10.1063/1.3356082.

[56] A. Valfells, L. K. Ang, Y. Y. Lau, and R. M. Gilgenbach, "Effects of an external magnetic field, and of oblique radio-frequency electric fields on multipactor discharge on a dielectric," *Phys. Plasmas*, vol. 7, no. 2, pp. 750–757, 2000, doi: 10.1063/1.873861.

[57] D.-Q. Wen, P. Zhang, Y. Fu, J. Krek, and J. P. Verboncoeur, "Temporal single-surface multipactor dynamics under obliquely incident linearly polarized electric field," *Phys. Plasmas*, vol. 26, no. 12, Dec. 2019, Art. no. 123509, doi: 10.1063/1.5126438.

[58] C. Chang *et al.*, "The influence of desorption gas to high power microwave window multipactor," *Phys. Plasmas*, vol. 15, no. 9, Sep. 2008, Art. no. 093508, doi: 10.1063/1.2977988.

[59] S. K. Nam and J. P. Verboncoeur, "Effect of electron energy distribution function on the global model for high power microwave breakdown at high pressures," *Appl. Phys. Lett.*, vol. 92, no. 23, Jun. 2008, Art. no. 231502, doi: 10.1063/1.2942382.

[60] S. K. Nam, C.-H. Lim, and J. P. Verboncoeur, "Dielectric window breakdown in oxygen gas: Global model and particle-in-cell approach," *Phys. Plasmas*, vol. 16, no. 2, Feb. 2009, Art. no. 023501, doi: 10.1063/1.3068746.

[61] Y. Y. Lau, J. P. Verboncoeur, and H. C. Kim, "Scaling laws for dielectric window breakdown in vacuum and collisional regimes," *Appl. Phys. Lett.*, vol. 89, no. 26, Dec. 2006, Art. no. 261501, doi: 10.1063/1.2425025.

[62] H. C. Kim and J. P. Verboncoeur, "Time-dependent physics of a single-surface multipactor discharge," *Phys. Plasmas*, vol. 12, no. 12, Dec. 2005, Art. no. 123504, doi: 10.1063/1.2148963.

[63] M. Siddiqi and R. A. Kishek, "Map-based multipactor theory for cross-field devices," *IEEE Trans. Electron Devices*, vol. 66, no. 7, pp. 3162–3167, Jul. 2019, doi: 10.1109/TED.2019.2914343.

[64] M. Siddiqi and R. A. Kishek, "A predictive model for two-surface multipactor stability and growth based on chaos theory," *Phys. Plasmas*, vol. 26, no. 4, Apr. 2019, Art. no. 043104, doi: 10.1063/1.5087586.

[65] M. Siddiqi and R. A. Kishek, "Construction of multipactor susceptibility diagrams from map-based theory," *IEEE Trans. Electron Devices*, vol. 66, no. 8, pp. 3587–3591, Aug. 2019, doi: 10.1109/TED.2019.2922147.

[66] *European Corporation for Space Standardization (ECSS), Space Engineering: Multipacting Design and Test*. ESA Publication Division. Accessed: 2013. [Online]. Available: http://everyspec.com/ESA/download.php?spec=ECSS-E-20-01A_REV-1.047803.pdf

[67] *Standard/Handbook for Multipactor Breakdown Prevention in Spacecraft Components (ANSI/AIAA S-142-2016)*, American Institute of Aeronautics and Astronautics, Reston, VA, USA, 2016, doi: 10.2514/4.104602.001.

[68] P. Y. Wong, P. Zhang, and J. P. Verboncoeur, "Harmonic generation in multipactor discharges," *IEEE Trans. Plasma Sci.*, vol. 48, no. 6, pp. 1959–1966, Mar. 2020, doi: 10.1109/TPS.2020.2980482.

[69] A. A. Hubble, P. T. Partridge, and R. Spektor, "Evolution of multipactor breakdown in two-tone systems," presented at the 9th Int. Workshop Multipactor, Corona, Passive Intermodulation, Noordwijk, The Netherlands, Apr. 2017.

[70] V. H. Chaplin, A. A. Hubble, K. A. Clements, and T. P. Graves, "Center conductor diagnostic for multipactor detection in inaccessible geometries," *Rev. Scientific Instrum.*, vol. 88, no. 1, Jan. 2017, Art. no. 014706, doi: 10.1063/1.4974346.

[71] T. P. Graves, P. Hanson, J. M. Michaelson, A. D. Farkas, and A. A. Hubble, "Fast shut-down protection system for radio frequency breakdown and multipactor testing," *Rev. Sci. Instrum.*, vol. 85, no. 2, Feb. 2014, Art. no. 024704, doi: 10.1063/1.4865403.

[72] P. T. Partridge and A. A. Hubble, "Multipactor phase null test diagnostic sensitivity and criteria," presented at the 9th Int. Workshop Multipactor, Corona, Passive Intermodulation, Noordwijk, The Netherlands, Apr. 2017.

[73] W.-C. Tang and C. M. Kudsia, "Multipactor breakdown and passive intermodulation in microwave equipment for stellite applications," in *Proc. IEEE Conf. Mil. Commun.*, Sep. 1990, pp. 181–187, doi: 10.1109/MILCOM.1990.117409.

[74] L. Zhang *et al.*, "Numerical simulation and analysis of passive intermodulation caused by multipaction," *Phys. Plasmas*, vol. 25, no. 8, Aug. 2018, Art. no. 082301, doi: 10.1063/1.5027061.

[75] V. E. Semenov, E. I. Rakova, N. A. Zharova, J. Rasch, D. Anderson, and J. Puech, "Simple model of the RF noise generated by multipacting electrons," *J. Phys. D: Appl. Phys.*, vol. 47, no. 5, Feb. 2014, Art. no. 055206, doi: 10.1088/0022-3727/47/5/055206.

[76] H. Yang, W. Huang, B. Zeng, and H. Wen, "An analytical method to evaluate the spectrum of multicarrier multipactor discharge," *IEEE Trans. Electron Devices*, vol. 68, no. 4, pp. 1918–1923, Apr. 2021, doi: 10.1109/TED.2021.3059808.

[77] S. A. Rice and J. P. Verboncoeur, "Migration of multipactor trajectories via higher-order mode perturbation," *IEEE Trans. Plasma Sci.*, vol. 45, no. 7, pp. 1739–1745, Jul. 2017, doi: 10.1109/TPS.2017.2704522.

[78] M. Siddiqi and R. Kishek, "A model for multipactor discharge on a dielectric based on chaos theory," *IEEE Trans. Electron Devices*, vol. 66, no. 10, pp. 4387–4391, Oct. 2019, doi: 10.1109/TED.2019.2932878.

[79] A. Iqbal, P. Y. Wong, D.-Q. Wen, S. Lin, J. Verboncoeur, and P. Zhang, "Time-dependent physics of single-surface multipactor discharge with two carrier frequencies," *Phys. Rev. E*, vol. 102, no. 4, p. 043201, Oct. 2020, doi: 10.1103/PhysRevE.102.043201.

[80] J. R. M. Vaughan, "Secondary emission formulas," *IEEE Trans. Electron Devices*, vol. 40, no. 4, p. 830, Apr. 1993, doi: 10.1109/16.202798.

[81] A. Iqbal, P. Y. Wong, J. P. Verboncoeur, and P. Zhang, "Frequency-domain analysis of single-surface multipactor discharge with Single- and dual-tone RF electric fields," *IEEE Trans. Plasma Sci.*, vol. 48, no. 6, pp. 1950–1958, Jun. 2020, doi: 10.1109/TPS.2020.2978785.

[82] D.-Q. Wen, A. Iqbal, P. Zhang, and J. P. Verboncoeur, "Suppression of single-surface multipactor discharges due to non-sinusoidal transverse electric field," *Phys. Plasmas*, vol. 26, no. 9, Sep. 2019, Art. no. 093503, doi: 10.1063/1.5111734.

[83] A. Iqbal, J. P. Verboncoeur, and P. Zhang, "Two surface multipactor discharge with two-frequency RF fields and space-charge effects," *Phys. Plasmas, Under Rev.*, 2021.

[84] P. Zhang, Á. Valfells, L. K. Ang, J. W. Luginsland, and Y. Y. Lau, "100 years of the physics of diodes," *Appl. Phys. Rev.*, vol. 4, no. 1, Mar. 2017, Art. no. 011304, doi: 10.1063/1.4978231.
[85] P. Zhang, Y. S. Ang, A. L. Garner, Á. Valfells, J. W. Luginsland, and L. K. Ang, "Space–charge limited current in nanodiodes: Ballistic, collisional, and dynamical effects," *J. Appl. Phys.*, vol. 129, no. 10, Mar. 2021, Art. no. 100902, doi: 10.1063/5.0042355.
[86] C. Watts, M. Gilmore, and E. Schamiloglu, "Effects of laser surface modification on secondary electron emission of copper," *IEEE Trans. Plasma Sci.*, vol. 39, no. 3, pp. 836–841, Mar. 2011, doi: 10.1109/TPS.2010.2102750.
[87] C. Chang *et al.*, "The effect of grooved surface on dielectric multipactor," *J. Appl. Phys.*, vol. 105, no. 12, Jun. 2009, Art. no. 123305, doi: 10.1063/1.3153947.
[88] M. Pivi, F. K. King, R. E. Kirby, T. O. Raubenheimer, G. Stupakov, and F. L. Pimpec, "Sharp reduction of the secondary electron emission yield from grooved surfaces," *J. Appl. Phys.*, vol. 104, no. 10, Nov. 2008, Art. no. 104904, doi: 10.1063/1.3021149.
[89] A. Iqbal *et al.*, "Empirical modeling and Monte Carlo simulation of secondary electron yield reduction of laser drilled microporous gold surfaces," *J. Vac. Sci. Technol. B, Microelectron.*, vol. 38, no. 1, Jan. 2020, Art. no. 013801, doi: 10.1116/1.5130683.
[90] J. Ludwick *et al.*, "Angular dependence of secondary electron yield from microporous gold surfaces," *J. Vac. Sci. Technol. B, Microelectron.*, vol. 38, no. 5, Sep. 2020, Art. no. 054001, doi: 10.1116/6.0000346.

Asif Iqbal (Member, IEEE) received the B.S. degree in electrical and electronic engineering from Bangladesh University of Engineering and Technology, Dhaka, Bangladesh, in 2015, and the Ph.D. degree in electrical engineering from Michigan State University, East Lansing, MI, USA, in 2021.

He is currently a Post-Doctoral Research Associate with the Department of Electrical and Computer Engineering, Michigan State University. His current research interests include analytical and Monte Carlo modeling of multipactor and secondary electron emission.

Dr. Iqbal was a recipient of the Michigan Institute of Plasma Science and Engineering (MIPSE) Graduate Fellowship Award from 2019 to 2020, the 2019 MIPSE Graduate Student Symposium Best Presentation Award, and the 2019–2020 Michigan State University Electrical Engineering Outstanding Graduate Student Award.

Patrick Y. Wong (Member, IEEE) received the B.S.E., M.S.E., and Ph.D. degrees from the University of Michigan, Ann Arbor, MI, USA, in 2013, 2015, and 2018, respectively.

He is currently a Post-Doctoral Researcher with the Department of Electrical and Computer Engineering, Michigan State University. His research interests include theoretical and computational modeling of beam–circuit interactions in high-power microwave devices including traveling-wave tubes, magnetrons, and multipactor.

De-Qi Wen (Member, IEEE) received the B.S. degree major in physics and minor in applied mathematics and the Ph.D. degree in plasma physics from Dalian University of Technology, Dalian, China, in 2012 and 2018, respectively.

In this period, he was jointly trained with the University of California, Berkeley, CA, USA, from 2015 to 2017. Since 2018, he has been a Post-Doctoral Researcher with the Department of Electrical and Computer Engineering and Department of Computational Mathematics Science and Engineering, Michigan State University. His research interests are multipactor, plasma ionization breakdown, electromagnetic waves, radio frequency plasma source including capacitive/inductive discharge especially in aspects of plasma series resonance, electromagnetic effects, sheath dynamics, electron dynamics, applicable to microwave devices and fabrication of semiconductor, through-code development/improvement such as particle-in-cell/Monte Carlo simulation (OOPD1, XPDP1, and XOOPIC, XPDC2 etc.), and development of new model and theory.

Dr. Wen has served as a Frequent Reviewer for more than ten internationally well-known journals such as the IEEE TRANSACTIONS ON PLASMA SCIENCE, *Journal of Applied Physics*, *Plasma Source Science and Technology*, *Applied Physics Letter*, *Journal of Physics D*: *Applied Physics*, *Plasma of Physics*, *Review of Scientific Instruments*, and so on.

John P. Verboncoeur (Fellow, IEEE) received the B.S. degree in engineering science from the University of Florida, Gainesville, FL, USA, in 1986, and the M.S. and Ph.D. degrees in nuclear engineering from the University of California at Berkeley (UCB), Berkeley, CA, USA, in 1987 and 1992, respectively.

He was a Post-Doctoral Researcher with the Lawrence Livermore National Laboratory, Livermore, CA, USA, and with the Department of Electrical Engineering and Computer Science (EECS), UCB. He was an Associate Research Engineer with EECS, UCB, where he was a Nuclear Engineering Faculty in 2001 and a Full Professor in 2008. From 2001 to 2010, he served as the Chair for the Computational Engineering Science Program, UCB. In 2011, he joined Michigan State University (MSU), East Lansing, MI, USA, as a Professor of electrical and computer engineering, where he was a Professor of computational mathematics, science, and engineering in 2015. He has authored or coauthored in MSU (formerly Berkeley) suite of particle-in-cell Monte Carlo codes, including XPDP1 and XOOPIC, used by more than 1000 researchers worldwide with more than 350 journal publications in the last decade, 350 journal articles and conference papers, with over 3500 citations, and has taught 13 international workshops and minicourses on plasma simulation. His current research interests include theoretical and computational plasma physics, with a broad range of applications spanning low-temperature plasmas for lighting, thrusters, and materials processing to hot plasmas for fusion, from ultracold plasmas to particle accelerators, from beams to pulsed power, from intense kinetic nonequilibrium plasmas to high-power microwaves.

Dr. Verboncoeur was a recipient of the Department of Energy (DOE) Magnetic Fusion Energy Technology Fellowship. He was a Past-President of the IEEE Nuclear and Plasma Science Society and an IEEE Director-Elect. He is currently an Associate Editor of the *Physics of Plasmas*. He has served as a Guest Editor and/or a Frequent Reviewer for the IEEE TRANSACTIONS ON PLASMA SCIENCE, the IEEE TRANSACTIONS ON ELECTRON DEVICES, and a number of other plasma and computational journals.

Peng Zhang (Senior Member, IEEE) received the B.Eng. and M.Eng. degrees in electrical and electronic engineering from Nanyang Technological University, Singapore, in 2006 and 2008, respectively, and the Ph.D. degree in nuclear engineering and radiological sciences from the University of Michigan (UM), Ann Arbor, MI, USA, in 2012.

He was an Assistant Research Scientist with the Department of Nuclear Engineering and Radiological Sciences, UM. He is currently an Associate Professor (an Assistant Professor, from 2016 to 2021) with the Department of Electrical and Computer Engineering, Michigan State University (MSU), East Lansing, MI, USA. He has authored or coauthored refereed journal publications on electrical contacts, thin films, classical, ballistic, and quantum diodes, space-charge-limited current flows, beam–circuit interaction, multipactor and breakdown, microwave absorption on rough surfaces, slow wave structures, z-pinches, laser–plasma interaction, and more recently on vacuum nanodevices, quantum tunneling plasmonic junctions, ultrafast photoemission, and novel miniaturized electromagnetic radiation sources. His current research interests include theoretical and computational physics in nanoelectronics, plasmas, and accelerator technology.

Dr. Zhang is currently serving as a member of the IEEE Plasma Science and Application (PSAC) Executive Committee and an Editorial Board Member for Scientific Reports and for Plasma Research Express. He was a Guest Editor of the 2020 Special Issue of the IEEE TRANSACTIONS ON PLASMA SCIENCE ON HIGH-POWER MICROWAVE AND MILLIMETER WAVE GENERATION. He was a recipient of the IEEE Nuclear and Plasma Sciences Society (NPSS) Early Achievement Award, the AFOSR Young Investigator Program Award, the ONR Young Investigator Program Award, the UM Richard and Eleanor Towner Prize for Outstanding Ph.D. Research, and the UM Rackham Presidential Fellowship Award.